International Journal of Solids and Structures 49 (2012) 584–589

Contents lists available at SciVerse ScienceDirect

International Journal of Solids and Structures

journal homepage: www.elsevier.com/locate/ijsolstr

Propagation of a cleavage crack front across a field of persistent grain boundaries

Weiyi Lu [a], Srinivas S. Chakravarthula [b], Jin Chen [a], Yu Qiao [a,*]

[a] Department of Structural Engineering, University of California – San Diego, La Jolla, CA 92093, USA
[b] Department of Civil Engineering, University of Akron, Akron, OH 44325, USA

ARTICLE INFO

Article history:
Received 15 November 2010
Received in revised form 20 October 2011
Available online 13 November 2011

Keywords:
Fracture toughness
Grain boundary
Cleavage
Nonuniform

ABSTRACT

The nonuniform propagation of a cleavage front across a field of persistent grain boundaries is analyzed. When a cleavage crack advances in a field of grains, some of the grain boundaries cannot be directly broken through, which interrupts the crack growth process. When the crack front bypasses such persistent grain boundaries (PGB), the overall crack growth driving force must be increased so that the local stress intensity can overcome the local fracture resistance. A theoretical model is developed based on the *R*-curve analysis. A closed-form expression of the critical stress intensity factor is given as a function of the line content of PGB.

1. Introduction

It has long been noticed that grain boundaries are important obstacles to cleavage crack propagation (Broberg, 1999; Crocker et al., 1996; Kanninen and Popelar, 1985). When the temperature is sufficiently low, the dominant fracture mode of an intrinsically brittle material is pure cleavage (McClintock and Argon, 1966; Hertzberg, 1995). The fracture is completed by separation of the most energetically favorable crystallographic planes. Due to the large stress concentration at the tip of a sharp crack, very often a cleavage front can easily advance across an entire crystal. For instance, even with river markings and small-scale yielding being taken into account, the effective surface free energy of the cleavage plane in a steel grain is typically only a few J/m^2 (Oura et al., 2010). To cleave a grain of the size around 10 μm, the fracture work is less than 1 nano-Joule.

As the cleavage front encounters a grain boundary, however, a significant amount of additional fracture work must be done. The first systematic study on this phenomenon was probably performed by Gell and Smith (1967), who noticed in a cryologically charged surface crack growth experiment that the probability of break-through of a grain boundary by a cleavage crack was dependent on both the twist and the tilt misorientation angles. Recently, Argon and Qiao (2002) and Qiao and Argon (2003a,b) carried out experiments on iron-silicon alloy single crystals and bicrystals. Based on the measurement results of the resistances of high-angle grain boundaries, a simple expression was derived to predict the grain boundary cleavage resistance:

$$\frac{G_{GB}}{G_A} = \frac{\sin\varphi + \cos\varphi}{\cos^2\psi} + C\frac{\sin\varphi\cos\varphi}{\cos\psi} \tag{1}$$

where G_{GB} and G_A are the fracture resistances of grain boundary and crystallographic plane, respectively; φ and ψ are the twist and the tilt misorientation angles across the grain boundary, respectively; and $C = 0.25$ is a material constant that collectively captures the effects of the crack front profile and the grain boundary shear strength. The crystallographic orientation comes in via a variety of mechanisms. First, as the cleavage facet deviates from the primary fracture plane, the area of fracture surface increases (Hull, 1999). Second, since the grain boundary needs to be separated apart, additional fracture work associated with the plastic shear and/or mode-II fracture must be done (McClintock, 1997). Third, a grain boundary is not broken through uniformly. The cleavage front always first penetrates stably across the boundary in a number of break-through windows, bowing into the next grain. The front sections in between the break-through windows are arrested at the boundary. Due to the nonuniform distribution of local stress intensity, the external loading must be higher than that of a straight crack front to drive the crack front to advance (Rice, 1985; Kong and Qiao, 2005). Finally, the grain boundary islands that bridge across the fracture flanks can result in local crack closure, causing a "post-cracking" toughening effect, somewhat similar with the short fibers in a composite material (Qiao et al., 2004). The combination of these factors may lead to various fracture appearances at grain boundaries, such as the regular mode, the irregular mode, and the mixed mode (Qiao, 2003, 2005a,b; Chen and Qiao, 2007), which are dependent on the chronology of the cracking process.

While the role of individual grain boundaries in cleavage crack propagation has been investigated intensively, the behaviors of a field of grains are still quite inadequately understood. In the

* Corresponding author.
E-mail address: yqiao@ucsd.edu (Y. Qiao).

0020-7683/$ - see front matter © 2011 Elsevier Ltd. All rights reserved.
doi:10.1016/j.ijsolstr.2011.11.003

Nomenclature

a	the effective crack length
b	the sample thickness
C_s	a geometrical factor taking account for the grain orientation
d	the grain size
D	the average center-to-center distance between persistent grain boundaries
E	the Young's modulus is the sample thickness, and h is the height of the DCB arm
$F(\xi_2)$	the pinning stress in a persistent grain boundary
G	the crack growth driving force
G_0	the reference fracture resistance of a polycrystalline material, where all the grain boundaries could be directly broken through by the crack front
G_A	the fracture resistances of crystallographic plane
G_{GB}	the fracture resistance of grain boundary
G_{PC}	the overall fracture resistance of a polycrystalline material
G_{PC0}	the reference fracture resistance of a polycrystalline material, where all the grain boundaries are type 1 or type 2
G_{cr}	the critical fracture resistance
$\widetilde{G}$	G_{PC}/G_0
h	the height of the arm of the double-cantilever beam sample
k^*	the mode II fracture resistance of the grain boundary
K	the average stress intensity factor along the crack front
K_{loc}	the local stress intensity factor
K_{cr}	the critical stress intensity factor
M	an internal variable for the pinning stress
P	crack opening load
R	the overall fracture resistance
t	the thickness of the grain boundary affected zone
U	the strain energy stored in the sample
$W\left(\vec{x}, \vec{\xi}\right)$	a weight function
$\widetilde{W}(\vec{x}, \vec{\xi})$	a weight function
$\vec{x} = (x, y)$	the global coordinate system
x	the axis of the global coordinate system parallel to the initial crack front
y	the axis of the global coordinate system parallel to the crack advance direction
y_0	the initial crack length
α_i	internal variables describing the crack front profile
$\hat{\alpha} \approx 3.17$	is a material constant related G_A to G_{PC0}
β_i	internal variables for the pinning stress
φ	the twist misorientation angle across a grain boundary
ψ	the tilt misorientation angle across a grain boundary
$\xi = (\xi_1, \xi_2)$	the local coordinate system, with the subscript "1" indicating the cleavage front direction and "2" indicating the crack advance direction
δ	the crack opening distance
δ_c	the preparatory opening displacement of the cracked planes across a boundary before the final boundary failure takes place
Δh	the half height difference of the cracked planes across a boundary before the final boundary failure takes place
Δy	the effective crack growth distance
Δy_{cr}	the critical crack growth distance
v	the Poisson's ratio
Ω	the domain of persistent grain boundary
ρ	$\left\|\vec{\xi} - \vec{\xi}\right\|$

simplest possible models where the grains are of regular shapes and sizes, each grain has at least 4 or 6 boundaries (Anderson et al., 1994; Crocker et al., 1996). When the crack front enters a grain from one side, it may either "spread" out into all the adjacent grains by breaking through other sides, or bypass some of the grains, leaving them behind. In some cases, the crack front may stop locally. Cracks arrested at grain boundaries have been repeatedly reported (Hahn et al., 1959; Mower and Argon, 1995; Chen et al., 2009), e.g. in the classic Griffith theory the presence of grain-sized microcracks is related to the initiation of global brittle failure of some engineering materials (Gdoutos, 2005).

If the two grains at either side of a boundary are cleaved, with the front advance directions either parallel or normal to the boundary, the boundary must be separated apart through a different process. In the case where the crack advance direction is parallel to the boundary, the boundary may serve as a bridging reinforcement component, which can be taken into consideration in the model developed by Andersson and Bergkvist (1970) or in the classic framework of area-average fracture work (e.g. Qiao and Kong, 2004; Bower and Ortiz, 1991). In a previous study (Qiao, 2005b), the accumulative fracture work of these grain boundaries was analyzed, according to which the overall fracture resistance can be calculated through

$$\widetilde{G} - 4\widetilde{G}^{1/4} = S^* \tag{2}$$

where $\widetilde{G} = G_{PC}/G_0$ and S^* is a parameter dependent on the grain size, the shear strength, the mode of crack front propagation, and the shear fracture process; G_{PC} is the overall fracture resistance; and G_0 is the reference fracture resistance if all the grain boundaries could be directly broken through by the crack front. However, the model assumes that all the grain boundaries along a cleavage front fail simultaneously, and, therefore, under-estimates the difference between a single crystal and its polycrystalline counterpart. If the crack advance direction is normal to the boundary, the propagation of the crack front would be interrupted as it encounters grain boundaries of different local fracture resistances and geometries.

2. Experimental

In order to investigate the cleavage cracking process in polycrystalline material, a 1020 steel was employed as a model material. The material was cut and milled into 50.8 mm by 254 mm plates, with the thickness of 6.2 mm. Double-cantilever beam (DCB) samples were produced by creating precracks along the longitudinal direction by electric discharge machining (EDM). The precrack length was around 120 mm. Precrack tips were sharpened by high-cycle fatigue. The DCB samples were thermally treated at 650 °C in nitrogen for 72 h, decarbonized at 600 °C in hydrogen for 10 min, and finally furnace cooled.

By using an Instron machine, a hardened steel wedge was compressed in between the two arms of the DCB sample. The wedge angel was 10°, and the crosshead speed was maintained constant at 0.5 mm/min. The bottom of the DCB sample was held firmly by a precision vise, with the edges of the jaws more than 100 mm away from the precrack tip. According to the Saint Venant's principle (Sadd, 2009), the boundary condition at the vise should not affect the crack tip behavior. The testing stage was kept in an environment chamber, with the temperature being controlled at −80 °C by using liquid nitrogen. The temperature variation in the chamber was less than ±5 °C, monitored by type-E thermocouples.

As the wedge was inserted, the DCB arms were forced apart, creating a crack growth driving force at the crack tip. Eventually,

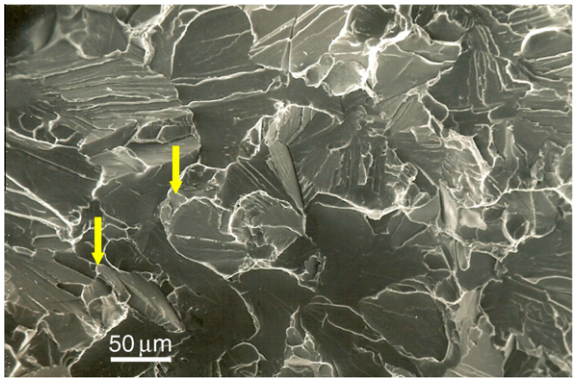

Fig. 1. SEM microscopy of the cleavage cracking process across a field of grains. The crack propagates from the left to the right. The persistent grain boundaries are indicated by the arrows.

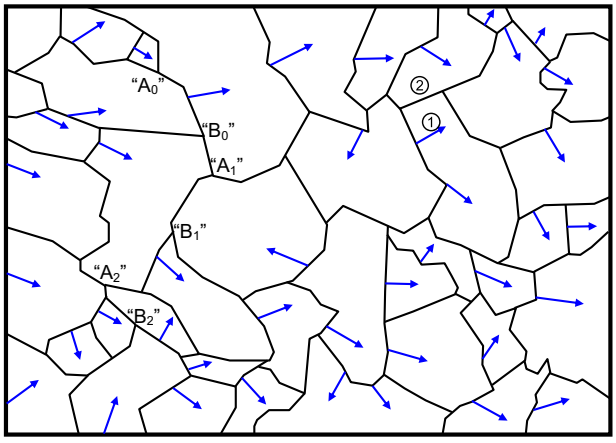

Fig. 2. The fracture map the of cleavage cracking process. The persistent grain boundaries are indicated as "A_1B_1" and "A_2B_2". The arrows indicate the local crack advance directions.

when the crack opening distance was sufficiently high, the crack would start to grow. Since the experiment was displacement controlled, the crack advance was quite jerky. Altogether, 5 samples were tested. The average fracture toughness was 18.4 MPa$\sqrt{\text{m}}$, with the standard deviation of 1.1 MPa$\sqrt{\text{m}}$.

The fracture surfaces were observed in a scanning electron microscope (SEM). Fig. 1 shows typical fractography. No evidence of plastic deformation associated with the separation of fracture surfaces inside grains could be detected. The crack propagation behavior in each grain was analyzed and a fracture map was developed, as shown in Fig. 2. According to the river markings and the extension of cleavage ledges, the local cracking direction at each grain boundary was identified and marked by the arrows.

3. Behaviors of persistent grain boundaries in cleavage cracking

From Figs. 1 and 2, it can be seen that there are three typical types of grain boundary behaviors when the crack advances across a field of grains. The first type of boundary, e.g. "A_0B_0", is parallel to the cleavage front. When the front reaches the boundary, it would be broken down into a number of terrains parallel to each other, along the cleavage plane of the grain ahead of the boundary. Such a geometrically necessary arrangement allows a smooth transition of fracture facets and minimizes the local fracture resistance (Qiao and Argon , 2003a), as shown in Eq. (1). The second type of boundary, such as the boundary between grains "①" and "②", are normal to the cleavage front. The crack front sections at either side of such a boundary advances quite independently, and the river markings in the two grains are somewhat symmetric. The front behavior at far field is similar to the near field, suggesting that the influence of the cracking process across the boundary is only secondary; that is, the separation of the grain boundary is not directly related to the crack front propagation.

If all the grain boundaries were type 1 and/or type 2, the overall fracture work of the field of grains, G_{PC0}, can be assessed by an equation developed by Qiao and Argon (2003c)

$$G_{\text{PC0}} = \hat{\alpha} \cdot G_{\text{A}} \tag{3}$$

where $\hat{\alpha} \approx 3.17$ is a material constant. For this equation, it is implicitly assumed that all the grain boundaries are uniformly separated apart. The fracture work of type 1 boundaries is captured by Eq. (1). The fracture work of type 2 boundaries is estimated as $d \cdot k^* \delta_c \Delta h$, where d is the grain size, k^* is the mode II fracture resistance of the grain boundary, and δ_c and Δh are the preparatory opening displacement and the half height difference of the cracked planes across the boundary before the final boundary failure takes place, respectively. In addition to the fracture work of grain boundaries, the fracture work of cleavage facets inside grains is assessed as $C_s \cdot G_A d^2/(\cos\varphi \cdot \cos\psi)$, with $C_s = 2/\sqrt{3}$ being a geometrical factor taking account for the fact that the fracture surface does not pass the main circles of all the grains. The value of $\hat{\alpha}$ reflects the average contributions of randomly oriented grains. For steel, with the additional fracture surface area associated with river markings and the small scale yielding being accounted for, the effective surface free energy of a cleavage plane is around $G_{\text{A}} = 10\,\text{J/m}^2$ (Boresi and Schmidt, 2002). Thus, according to Eq. (3), the cleavage resistance of a polycrystalline steel should be about 32 J/m^2, corresponding to a fracture toughness of 2.7 MPa$\sqrt{\text{m}}$, which is smaller than the measured data by almost an order of magnitude.

Type 1 and type 2 represent two extreme conditions. A detailed analysis of the fracture surfaces indicates that there exists a third type, as marked by the arrows in Fig. 1 and "A_1B_1" and "A_2B_2" in Fig. 2. The failure of such a grain boundary exhibits mixed characteristics: a part of the grain boundary is broken through by the cleavage front, accompanied with the formation of river markings; the rest of the boundary is separated through shear or secondary cracking, showing evidences of smearing and/or plastic bending of ligaments. For instance, similar to the first type of boundary, "A_1B_1" and "A_2B_2" are parallel to the cleavage front. However, when the front reaches them, it is locally arrested. The boundaries are separated apart after the rest of front sections pass across the grains ahead of them. That is, they have been left behind the verge of propagating front and bridged across the fracture flanks. This type of grain boundaries will be referred to as persistent grain boundaries (PGBs) in the following discussion.

Fig. 3 depicts a two dimensional simplification of the front propagation process around a PGB. As the regular grain boundaries are broken through by the cleavage front, the protruding parts of the front bow around the PGB, with an effective crack growth distance of Δy. The PGB pins the two fracture flanks together, and, thus, there must be a pinning stress, $F(\xi_2)$, in the PGB, where $\xi = (\xi_1, \xi_2)$ is the local coordinate system. The origin of ξ is at the middle point of the PGB, with the subscript "1" indicating the cleavage front direction and "2" indicating the crack advance direction. The pinning stress affects the local stress intensity at the crack front. At the protruding section in between PGBs, the crack growth driving force, G, would be lowered; the local G at the PGB tends to be higher. In order to keep the local stress intensity equal to the local fracture toughness, the overall crack growth driving force should be larger. This toughening effect, which is associated with the nonuniform nature of cleavage front propagation around PGBs, is not considered in Eq. (3).

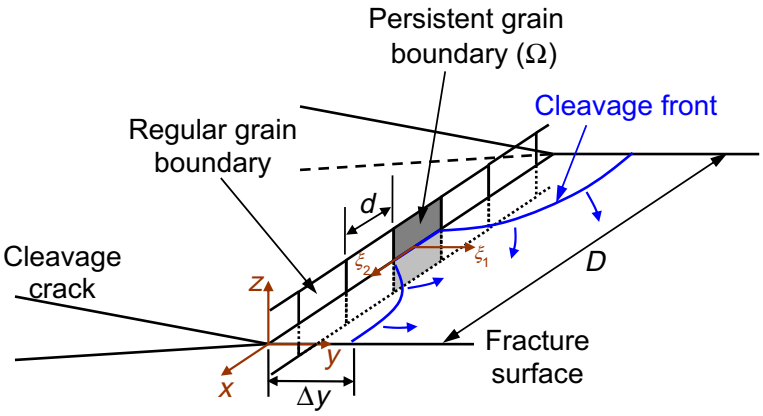

Fig. 3. Schematic of cleavage cracking across a field of grains.

The formation of PGB can be related to the variations of local stress intensity and local fracture resistance. From Eq. (1), it can be seen that if the twist misorientation across a boundary is large, the grain boundary toughness can be much higher than the average value. As will be clear shortly, when the cleavage front is curved, the local crack growth driving force at the protruding part is considerably lower than that at the concave sections. As a result, if a cleavage front section of a relatively low local stress intensity reaches a grain boundary of a relatively high local fracture resistance, direct breakthrough may be difficult and the front section can be arrested. Such a boundary becomes a PGB, which significantly promotes the nonuniform characteristics of the cleavage front behavior.

4. *R*-curve analysis for persistent grain boundary

As the crack front penetrates in between PGBs, the effective crack length increases. When a pair of crack opening loads, P, are applied by the wedge on the DCB specimen, the crack opening distance, δ, can be calculated in the framework of basic beam theory: $\delta = 8Pa^3/Ebh^3$, where $a = y_0 + \Delta y$ is the effective crack length, y_0 is the initial crack length, E is the Young's modulus, b is the sample thickness, and h is the height of the DCB arm. The strain energy stored in the sample can be assessed as

$$U = \frac{4P^2a^3}{Ebh^3} = \frac{\delta^2 Ebh^3}{16a^3} \tag{4}$$

With a constant crack opening load, the overall crack growth driving force is

$$G = -\frac{1}{b}\frac{\partial U}{\partial a}\bigg|_{\delta} = \frac{12P^2a^2}{Eb^2h^3}, \tag{5}$$

The average stress intensity factor along the crack front can then be estimated as

$$K = \sqrt{\frac{EG}{1-\nu^2}} = \frac{Pa}{bh}\sqrt{\frac{12}{(1-\nu^2)h}} \tag{6}$$

with ν being the Poisson's ratio. The changing rate of the crack growth driving force with respect to the crack length is

$$\frac{\partial G}{\partial a} = \frac{24P^2a}{Eb^2h^3} = \frac{2G}{a} \tag{7}$$

As depicted in Fig. 3, after the cleavage front encounters a PGB, even if initially it is straight, its propagation becomes nonuniform. The regular grain boundaries in between adjacent PGBs are directly broken through, while the front section at the PGB is arrested. To keep the crack opening distance at the PGB zero, the pinning stress must satisfy (Xu et al., 1998)

$$\int_{\Omega} W(\vec{x},\vec{\xi})F(\xi_2)\,d\Omega = \sqrt{\frac{2E\Delta y}{\pi(1-\nu^2)}}R \tag{8}$$

where Ω denotes the domain of PGB ($-\Delta y - t/2 \leqslant \xi_1 \leqslant -\Delta y + t/2$ and $-d/2 \leqslant \xi_2 \leqslant d/2$), with t being the thickness of grain boundary affected zone; R is the overall fracture resistance offered by the PGB; and

$$W\left(\vec{x},\vec{\xi}\right) = \frac{1}{\rho\pi^2}\arctan\left\{2\sqrt{|\xi_1 y|}/\rho\right\}$$

is a weight function, with $\rho = \left|\vec{x}-\vec{\xi}\right|$ and $\vec{x} = (x,y)$ being a global coordinate system with the origin at the center point of the regular grain boundary array between two adjacent PGBs. The x axis is parallel to the initial cleavage front and y is along the crack advance direction. The left-hand side of Eq. (8) reflects the crack closure displacement caused by the pinning stress, and the right-hand side is the crack opening displacement if the pinning stress were zero. The balance of the two sides should be met for every $\vec{x} = (x,0)$ in Ω.

The pinning stress would significantly affect the local stress intensity along the penetrating crack front. At the steady-state, the local stress intensity factor, K_{loc}, equals to the local fracture toughness. Since the regular grain boundaries in between PGBs can be classified as either type one or type two, the resistance that they offer to the cleavage front can be described by Eq. (2). Therefore, $K_{\mathrm{loc}} = \sqrt{EG_{\mathrm{PC0}}/(1-\nu^2)}$. The local stress intensity is determined by both the remote crack opening load, P, and the near-field pinning stress, F. Thus, for $\vec{x}$ at the front section propagating across the regular grain boundaries

$$\sqrt{\frac{ER}{1-\nu^2}} - \int_{\Omega}\widetilde{W}\left(\vec{x},\vec{\xi}\right)F(\xi_2)d\Omega = \sqrt{\frac{EG_{\mathrm{PC0}}}{1-\nu^2}} \tag{9}$$

where

$$\widetilde{W}\left(\vec{x},\vec{\xi}\right) = \sqrt{\frac{2}{\pi^3}}\frac{\sqrt{|y-\Delta y|}}{(x-\xi_2)^2+(y-\Delta y)^2}$$

is a weight function. The first term at the left-hand side captures the contribution of the far-field loading, and the second term reflects the contribution of the pinning stress. The profile of the penetrating crack front may be taken as a Nth order polynomial: $y = \Delta y + \sum_{i=1}^{N}\alpha_i x^i$ for $-(D-d)/2 \leqslant x \leqslant (D-d)/2$, where D is the average center-to-center distance between PGBs and α_i are coefficients to be determined.

When a crack opening load (P) is applied, the overall crack growth driving force, G, can be calculated through Eq. (5) as a function of the effective crack growth distance, Δy. With a given Δy, the combination of Eqs. (8) and (9) gives the overall fracture

resistance, R, with the byproduct of the solution of the pining stress, $F(\xi_2)$. At the equilibrium,

$$G = R \tag{10}$$

through which the value of Δy can be determined. That is, as a crack growth driving force G, which should be higher than G_{PC0} so that the crack front can overcome the resistance of the regular grain boundaries, is applied, the crack front bows in between the PGBs. As the effective crack length increases, according to Eq. (9), the local crack growth driving force at the verge of propagating front keeps decreasing. Eventually, at Δy, Eq. (10) is satisfied and the crack growth would cease. Under this condition, if Δy further increases, both G and R become larger.

The changing rate of G is given by Eq. (7), which is proportional to a^2. By taking first-order derivatives of both sides of Eqs. (8) and (9) with respect to a, we have

$$\int_\Omega \left[\frac{\partial W\left(\vec{x}, \vec{\xi}\right)}{\partial a} F(\xi_2) + W\left(\vec{x}, \vec{\xi}\right) \frac{\partial F(\xi_2)}{\partial a} \right] d\Omega = \frac{1}{2} \left(\frac{2E\Delta y}{\pi(1-\nu^2)} R \right)^{-\frac{1}{2}} \left(R + \Delta y \frac{\partial R}{\partial a} \right) \tag{11}$$

and

$$\frac{1}{2} \left(\frac{ER}{1-\nu^2} \right)^{-\frac{1}{2}} \frac{\partial R}{\partial a} = \frac{\partial}{\partial a} \left[\int_\Omega \widetilde{W}\left(\vec{x}, \vec{\xi}\right) F(\xi_2) d\Omega \right] \tag{12}$$

respectively. The combination of Eqs. (11) and (12) gives the value of $\partial R/\partial a$ as a function of Δy. Through the numerical solution that will be discussed shortly, as a rises, $\partial R/\partial a$ is positive but decreases as a increases. Initially, when the cleavage front just begins to penetrate across the PGBs, the value of Δy is small. Under this condition, $\partial G/\partial a < \partial R/\partial a$. Thus, when the equilibrium condition of $G = R$ is reached, further increase in a would lead to a smaller crack growth driving force than the overall fracture resistance, so that the crack growth is stable. The external loading, P, must be increased to maintain the cleavage front advancing. As Δy becomes larger, $\partial G/\partial a$ keeps rising while $\partial R/\partial a$ keeps decreasing. Eventually, at the critical crack growth distance, Δy_{cr},

$$\partial G/\partial a = \partial R/\partial a \tag{13}$$

At Δy_{cr}, an infinitesimal increase in a would cause $\partial G/\partial a > \partial R/\partial a$, so that the fracture resistance is insufficient to stop the crack, as depicted in Fig. 4. Consequently, the crack advance becomes unstable and the final failure of the material takes place. Such an R-curve analysis method has been employed to explain numerous experimental results (e.g. Freund, 1998). Once Δy_{cr} is obtained by solving Eqs. (10) and (13), the critical fracture resistance, G_{cr}, can be calculated via Eq. (5). It is the highest resistance that the material can offer to the cleavage crack.

5. Results and discussion

With a given d/D ratio, G_{cr} can be calculated by solving Eqs. (5) and (7)–(13). In the current study, the Ritz method was employed. It was assumed that the pinning stress can be expressed as $F(\xi_2) = \sum_{j=0}^{M} \beta_j \xi_2^j$, with M and β_i being parameters to be determined. By substituting the expression of the pinning stress in Eqs. (8) and (11), the integral equations can be reduced to a set of algebra equations of α_i. Similarly, Eqs. (9) and (12) can be reduced to algebra equations of β_j. According to the experimental measurement, the grain size (d) was taken as 80 μm; E and ν were set to 211 GPa and 0.28, respectively; y_0 was taken as 120 mm; and b and h were set to 6.2 mm and 25 mm, respectively. Note that the model is scalable and the geometrical parameters come in by affecting G, which is a part of the solution. The elastic properties, E and ν, are used in the equations to relate the stress intensity factor to the fracture resistance, which are equivalent to each other under the small scale yielding assumption. If the term of pinning stress in Eqs. (8) and (9) is redefined as $\sqrt{\frac{1-\nu^2}{E}} F(\xi_2)$, while mathematically the equations are the same, the influence of the parameters of E and ν would vanish.

The numerical results are shown in Fig. 5: the critical stress intensity factor, K_{cr}, increases monotonically with d/D, as it should, since d/D reflects the line content of PGBs. If the grain size is constant, as the d/D ratio increases, the distance between adjacent PGBs decreases; that is, the density of PGBs becomes larger. If the value of D is fixed, a higher d/D ratio indicates a larger d, so that the effect of each PGB is more pronounced. The numerical solution can be regressed as

$$\frac{K_{cr}}{K_{PC0}} = \sqrt{\frac{G_{cr}}{G_{PC0}}} = 1 + \lambda_1 \frac{d}{D} + \lambda_2 \left(\frac{d}{D} \right)^2 \tag{14}$$

where $\lambda_1 = 49$ and $\lambda_2 = 306$; $K_{PC0} = \sqrt{EG_{PC0}/(1-\nu^2)}$; and $K_{cr} = \sqrt{EG_{cr}/(1-\nu^2)}$ is the critical stress intensity factor.

According to the fractography analysis, about 9% of the grains in the material under investigation have PGBs. Thus, the line content of PGBs along the cleavage front, d/D, is nearly 0.09. At this d/D ratio, K_{cr}/K_{PC0} is about 8. As discussed previously, if K_{PC0} is assessed as

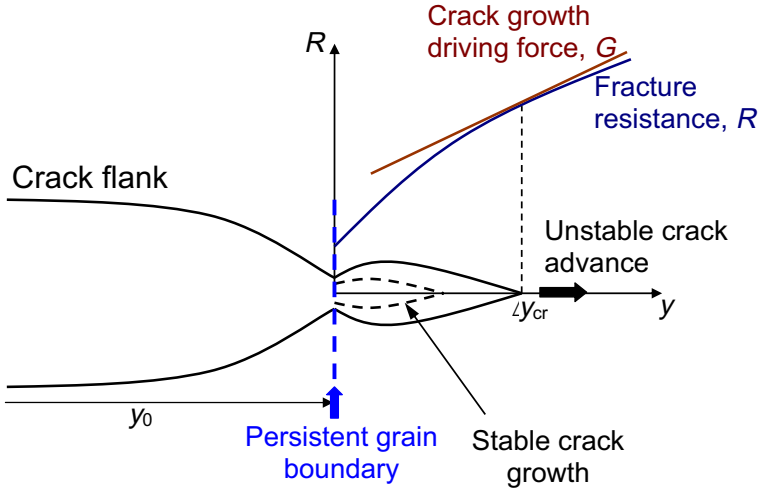

Fig. 4. Schematic of the R-curve.

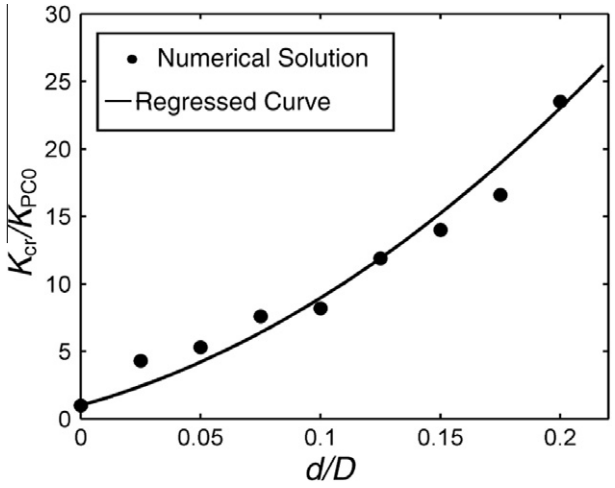

Fig. 5. The maximum fracture resistance, G_{cr}, as a function of d/D.

2.7 MPa$\sqrt{m}$, the value of K_{cr} should be 21 MPa$\sqrt{m}$, higher than but close to the measured critical stress intensity factor of 18.4 MPa$\sqrt{m}$, which looks plausible. The 15% difference between the numerical prediction and the testing result may be attributed to the simplicity of the assumptions of the model. First, the grain size inevitably exhibits a certain distribution. It is noticed that the probability for a larger grain to be a PGB is lower, probably because a wider grain boundary can provide more "weak" sites for a cleavage front to break through. Since PGBs tend to be the smaller grains, their average width would be smaller than the average grain size, d. Second, the PGBs do not distribute uniformly in the fracture surface. In some areas they are farther apart from each other, compared with other areas. If the local line content of PGBs is small, they provide a smaller resistance to the crack advance, which may become a "weakest link" in the material. Since the fracture toughness is governed by the weakest component, no matter how tough other areas would be, the overall fracture toughness tends to be lower than the prediction based on the average values. Third, it has been noticed in the experiment that, around the toughest grain boundaries, the crack front may turn back locally and join up with the front sections left behind. Such PGBs become ligaments that bridge the fracture flanks together, which is not considered in the above discussion.

The dominant factors of whether a grain boundary is a PGB or a regular boundary are still under investigation. It is envisioned that, if the PGB formation is dominated by the local grain boundary toughness, which is governed by the crystallographic misorientations (Eq. (1)), in materials where the grains are randomly oriented, the content of PGB should be the same (~9%). For materials that work under anisotropic loadings, there may exist optimum textures, with which, when the direction of the highest cracking resistance is aligned with the external loading, the PGB formation can be promoted and the effective material toughness can be maximized. The formation of PGBs is also related to the crack front profile. If the microstructure of the material is designed so that the uniform crack front advance is appropriately interrupted, the grain boundaries exposed to the concave sections of the crack front may tend to become persistent ones.

6. Concluding remarks

In a fractography study, three types of grain boundary behaviors in cleavage cracking in a polycrystalline material were identified. The first is the direct break-through of cleavage front across the boundary. The second is the separate failure parallel to the crack advance direction. In these two types of behaviors, the failure of grain boundaries along the cleavage front is simultaneous, and the crack front advance is relatively uniform. The third type of grain boundary behavior involves delayed boundary separation. Such a persistent grain boundary would cause nonuniform crack front propagation, which, due to the reduction in local stress intensity at the protruding parts of the crack front, provides a toughening mechanism. An R-curve analysis shows that this model can explain the large resistance offered by a field grains to cleavage cracking. A Ritz method was used to solve the equations numerically, and a closed-form expression was obtained.

Acknowledgement

This work was supported by the Department of Energy under Grant No. DE-FG02-07ER46355.

References

Anderson, T.L., Stienstra, D., Dodds Jr., R.H., 1994. In: Landes, J.D., McCabe, D.E., Boulet, J.A.M. (Eds.), Fracture Mechanics, ASTM STP-1207, vol. 24. ASTM, Philadelphia, PA, p. 186.
Andersson, H., Bergkvist, H., 1970. J. Mech. Phys. Solids 18, 1.
Argon, A.S., Qiao, Y., 2002. Resistance of cleavage cracking of high-angle bicrystal grain boundaries in Fe-Si alloy. Phil. Mag. A 82, 3333–3348.
Boresi, A.P., Schmidt, R.J., 2002. Advanced Mechanics of Materials. Wiley.
Bower, A.F., Ortiz, M., 1991. A three dimensional analysis of crack trapping and bridging by tough particles. J. Mech. Phys. Solids 39, 815–858.
Broberg, K.B., 1999. Cracks and Fracture. Academic Press.
Chen, J., Qiao, Y., 2007. Mixed-mode cleavage front branching at a high-angle grain boundary. Scrip. Mater. 56, 1027–1030.
Chen, J., Lu, W., Qiao, Y., 2009. Resistance of grain boundary array to cleavage cracking in free-standing thin film. Mech. Mater. 41, 131–138.
Crocker, A., Smith, G., Flewitt, P., Moskovic, R., 1996. In: Proceedings of the 11th European Conference on Fracture (ECF11). Eng. Mater. Advis. Serv., Warley, UK, vol. 1, p. 233.
Freund, L.B., 1998. Dynamic Fracture Mechanics. Cambridge University Press.
Gdoutos, E.E., 2005. Fracture Mechanics. Springer.
Gell, M., Smith, E., 1967. The propagation of cracks through grain boundaries in polycrystalline 3% silicon-iron. Acta Mett. 15, 253–258.
Hahn, G.T., Averbach, B.L., Owen, W.S., Cohen, M., 1959. In: Averbach, B.L., Felbeck, D.K., Hahn, G.T., Thomas, D.A. (Eds.), Fracture. MIT Press, Cambridge, MA, p. 91.
Hertzberg, R.W., 1995. Deformation and Fracture Mechanics of Engineering Materials. Wiley.
Hull, D., 1999. Fractography. Cambridge University Press.
Kanninen, M.F., Popelar, C.H., 1985. Advanced Fracture Mechanics. Oxford University Press.
Kong, X., Qiao, Y., 2005. Crack trapping effect of persistent grain boundary islands. Fatigue Fract. Eng. Mater. Struct. 28, 753–758.
McClintock, F.A., 1997. A three dimensional model for polycrystalline cleavage and problems in cleavage after extended plastic flow or cracking. In: Chan, K.S., George, R. (Eds.), Irwin Symposium on Cleavage Fracture. TMS. pp. 81–94.
McClintock, F.A., Argon, A.S., 1966. Mechanical Behaviors of Materials. Addison-Wesley.
Mower, T.M., Argon, A.S., 1995. Mech. Mater. 19, 343.
Oura, K., Lifshits, V.G., Saranin, A.A., Zotov, A.V., Katayama, M., 2010. Surface Science. Springer.
Qiao, Y., 2003. Modeling of resistance curve of high-angle grain boundary in Fe-3wt%Si alloy. Mater. Sci. Eng. A 361, 350–357.
Qiao, Y., 2005a. Irregular-mode cracking in Fe-3wt.%Si alloy. J. Mater. Sci. Tech. 21, 338–342.
Qiao, Y., 2005b. The role of recalcitrant grain boundaries in cleavage cracking in polycrystals. J. Mater. Sci. 40, 4819–4825.
Qiao, Y., Argon, A.S., 2003a. Cleavage cracking resistance of high angle grain boundaries in Fe-3wt%Si alloy. Mech. Mater. 35, 313–331.
Qiao, Y., Argon, A.S., 2003b. Brittle-to-ductile fracture transition in Fe-3wt%Si single crystals by thermal crack arrest. Mech. Mater. 35, 903–912.
Qiao, Y., Argon, A.S., 2003c. Cleavage crack-growth-resistance of grain boundaries in polycrystalline Fe-2wt%Si alloy: experiments and modeling. Mech. Mater. 35, 129–154.
Qiao, Y., Kong, X., 2004. An energy analysis of the grain boundary behavior in cleavage cracking in Fe-3wt.%Si alloy. Mater. Lett. 3156-3160 (2004).
Qiao, Y., Kong, X., Pan, E., 2004. Fracture toughness of thermoset composites reinforced by perfectly bonded impenetrable short fibers. Eng. Fract. Mech. 71, 2621–2633.
Rice, J.R., 1985. First-order variation in elastic fields due to variation in location of a planar crack front. J. Appl. Mech. 52, 571–579.
Sadd, M.H., 2009. Elasticity. Academic Press.
Xu, G., Bower, A.F., Ortiz, M., 1998. The influence of crack trapping on the toughness of fiber reinforced composites. J. Mech. Phys. Solids 46, 1815–1833.